Nuclear Data for Science and Technology (1988 MITO), 603- 606, Copyright © 1988 JAERI.

# CALCULATION OF $^{235}U(n,n')$ CROSS SECTIONS FOR ENDF/B-VI

P. G. Young and E. D. Arthur

Los Alamos National Laboratory, Los Alamos, New Mexico, USA

**Abstract**: Cross sections for neutron-induced reactions on $^{235}U$ between 0.01 and 20 MeV have been calculated in a preliminary analysis for the ENDF/B-VI evaluation, with particular emphasis on neutron inelastic scattering. A deformed optical model potential that fits total, elastic, inelastic, and low-energy average resonance data is used to calculate direct (n,n') cross sections and transmission coefficients for a Hauser-Feshbach statistical theory analysis using a multiple fission barrier representation. Direct cross sections for higher-lying vibrational states are provided from DWBA calculations, normalized using $B(E\ell)$ values determined from (d,d') and Coulomb excitation data. Initial fission barrier parameters and transition state density enhancements appropriate to the compound systems involved were obtained from previous analyses, especially fits to charged-particle fission probability data. Further modifications to fit $^{235}U(n,f)$ data were small, and the final fission parameters are generally consistent with published values. The results from this preliminary analysis are compared with the ENDF/B-V evaluation as well as with experimental data.

(Keywords: $^{235}U$, neutron reactions, data evaluation, nuclear models, coupled-channel optical model, fission theory)

## Introduction

The current ENDF/B-V.2 evaluation of $n+^{235}U$ inelastic neutron, (n,2n), and (n,3n) data is based on the 1973 evaluation by Stewart et al.,[1] which was incorporated into ENDF/B-IV. Since that time, limited new experimental data have become available and, especially, major advances have been made in nuclear theory codes that permit more reliable calculation of neutron emission data. For example, the neutron scattering, (n,2n), and (n,3n) data in the existing ENDF/B-V.2 evaluation for $n+^{239}Pu$ was significantly improved over earlier evaluations by utilizing a modern theoretical analysis.[2] The results for $^{239}Pu$ demonstrably improved agreement of calculations with fast critical experiments that are sensitive to neutron spectra.[2] The present calculations were undertaken to provide a similar framework for improving the neutron emission data in the upcoming $n+^{235}U$ evaluation for ENDF/B-VI.

## Theoretical Analysis and Results

The basic components of our theoretical calculations are described in earlier analyses[2,3] of neutron interactions with $^{239}Pu$ and $^{238}U$. The present analysis involves application of four main reaction models: a coupled-channel optical model to describe direct-reaction contributions to inelastic scattering from the ground state rotational band; Hauser-Feshbach statistical theory to calculate compound-nucleus contributions to the reactions; distorted-wave Born approximation (DWBA) calculations for (uncoupled) members of $^{235}U$ vibrational bands; and, a multiple-barrier fission model to describe the fission channels that compete with neutron and gamma-ray emission. The neutron transmission coefficients required for the Hauser-Feshbach calculations were obtained from the coupled-channel analysis, thereby ensuring consistency between the compound-nucleus and the main direct-reaction parts of the calculations. Above an incident neutron energy of ~10 MeV, an exciton preequilibrium model was used to correct the statistical theory calculations for nonequilibrium effects.

### Deformed Optical Model

The coupled-channel deformed optical model calculations were performed with the ECIS computer code.[4] The first three states in the $^{235}U$ ground state rotational band ($7/2^-$, $9/2^-$, $11/2^-$) were coupled in the calculation. A standard form was used for the optical model potential,[5] and the coupling form factors needed in the expansion of the optical parameters were assumed complex. Initial values for the neutron optical parameters were obtained from the analysis of Haouat et al.,[6] which relied mainly on fits to total, elastic, and inelastic cross sections as well as s- and p-wave neutron strength functions. Modifications were made to the Haouat parameters to enhance agreement with total cross section measurements near 1 MeV,[7] and to extend the parameterization to a neutron energy of 30 MeV. The resulting optical model and deformation parameters are given in Table 1. The neutron total cross section calculated with this potential is compared to experimental data[8] in Fig. 1.

### Hauser-Feshbach Statistical Theory

For incident neutron energies below 5 MeV, the Hauser-Feshbach statistical theory calculations were performed with the reaction theory code COMNUC,[9] which includes width-fluctuation corrections. At higher neutron energies the GNASH[10] code was used, with preequilibrium corrections incorporated above $E_n$ ~10 MeV. The phenomenological level density model of Gilbert and Cameron,[11] together with the parameters of Cook et al.,[12] were used to describe continuum level densities. The continuum level densities were matched with the experimental level data for each residual nucleus in the calculations, so as to reproduce the cumulative number of levels at low excitation energy while joining smoothly to the Fermi-gas formulation at higher energy.

Transmission coefficients for gamma rays were calculated using a giant-dipole-resonance expression,[13] utilizing two Lorentzian forms to represent the split giant dipole resonance. The gamma-ray strength function was normalized using $2\pi\langle\Gamma_\gamma\rangle / \langle D\rangle$ values obtained from resonance data with s-wave neutrons. The strength function that resulted was used for all compound systems in the calculation.

The calculated elastic and inelastic scattering angular distributions are compared in Fig. 2 with measurements by Haouat et al.[6] at 0.7 MeV and in Fig. 3 with Haouat's measurements at 3.4 MeV. Due to the close spacing of levels in $^{235}U$, the "elastic" angular distributions also contain (n,n') contributions to the lowest $1/2^+$ and $3/2^+$ excited states, and similarly the $9/2^-$ and $5/2^+$ states were not resolved in the inelastic distributions. At 3.4 MeV, the coupled-channel direct reaction components dominate, but at 0.7 MeV the compound-nucleus components are still significant. Overall the agreement of the calculations with the experimental data appears reasonable.

The integrated elastic scattering and low-lying inelastic level cross sections are compared to measurements by Smith and Guenther[14] in Table 2. Again, because of the close spacing of levels in $^{235}U$, the elastic measurement was not resolved from the lowest excited levels, so we summed the (n,n') cross sections up to an excitation energy $E_x$ (see Table II) with the elastic cross section to compare with this measurement. The calculated results, which are dominated by the ground state rotational band, are reasonably consistent with the measurement although they appear to fall at the lower edge of the error bar on the data. An exception is the calculation at the lowest energy (0.93 MeV), which lies four standard deviations below the data. This result appears balanced to some extent by the agreement of the calculation at 0.7 MeV with the measurements of Haouat et al.[6] shown in Fig. 2.

DWBA Calculations

Although most of the direct reaction contribution to inelastic scattering is provided by the coupled-channel calculations of the ground state rotational band (corresponding to the $9/2^-$ and $11/2^-$ excited states at excitation energies of 46.2 and 103.0 keV), additional contributions can come from vibrational states, generally lying at higher excitation energies. Because of the close spacing of levels in $^{235}U$, experimental information on (n,n') reactions to such vibrational states is essentially nonexistent. Therefore, to account for such contributions, we performed DWBA calculations on the even-even target nuclei $^{234}U$ and $^{238}U$, using reduced transition probabilities $B(E\ell)$ from (d,d') and Coulomb excitation measurements[15] to obtain absolute (n,n') cross sections and a weak coupling model[16] to apply the results to states in $^{235}U$. The $B(E\ell)$ values for $^{234}U$, which are more appropriate for applying this model to $^{235}U$, appear to be of the order of 40% larger than for $^{238}U$. We considered the $^{238}U$ data because the amount of information is somewhat greater in this case.

The strongest transitions observed in $^{234}U(d,d')$ and $^{238}U(d,d')$ measurements involve population of $3^-$ and $2^+$ vibrational states, corresponding to angular momentum transfers of $\ell=3$ and $\ell=2$, respectively. The sum of $^{235}U(n,n')$ cross sections calculated from the dominant $\ell=3$ and $\ell=2$ transitions amounts to approximately 10% of the coupled-channel direct reactions at a neutron energy of 3 MeV, 30% at 8 MeV, and 23% at 20 MeV. While these direct contributions are not large, they do lead to a hardening of the inelastic neutron spectrum and will be included in the ENDF/B-VI evaluation.

Fission Channel

Although we are relying on experimental data for the total fission cross section in the actual evaluation, it is essential to calculate the fission channel reliably because it provides an important constraint on the Hauser-Feshbach calculations of the (n,n'), (n,2n), and (n,3n) reactions. In our calculations with both COMNUC and GNASH, we utilize a double-humped barrier model with two uncoupled oscillators for the barrier representation. Under these circumstances the total fission transmission coefficient for a given compound nucleus state of energy E, spin J, and parity $\pi$ is given by

$$T_F(E,J,\pi) = \frac{N_A(E,J,\pi)N_B(E,J,\pi)}{N_A(E,J,\pi) + N_B(E,J,\pi)} . \qquad (1)$$

The subscripts A and B refer to the inner and outer barriers, respectively. The quantity $N_A$ (and similarly $N_B$) is given by

$$N_A(E,J,\pi) = \sum_{\upsilon} P_A^{\upsilon}(E,J,\pi) + \int \frac{\rho_A(\epsilon,J,\pi)\, d\epsilon}{\exp[2\pi(E_A + \epsilon - E)/\hbar\omega_A]} , \qquad (2)$$

where the first term represents a sum over discrete fission transition states whose fission penetrability is calculated using a Hill-Wheeler expression.[17] The second term represents the integral over the contributions from the continuum of such states, where again the fission penetrability is determined using a Hill-Wheeler form. The quantities $E_A$ and $\hbar\omega_A$ represent the height and curvature associated with the fission barrier of interest.

For each fissioning system we constructed the spectrum of transition states occurring at each barrier from the available bandhead information. We again assumed the Gilbert-Cameron level density form to represent the continuum of fission transition states, using parameters applicable to the ground-state deformation case. Because of symmetry conditions existing at the individual barriers, this procedure is not appropriate to describe the actual density of transition states. To correct for symmetry effects, we included enhancement factors that directly multiply the level densities calculated for ground-state deformations.

Initial fission barrier heights and values for $\hbar\omega$ were obtained from analyses of (t,pf) data.[18] We took general guidance for the form of the level density enhancements from the work of Bjørnholm et al.,[19] although they were adjusted along with the fission barrier heights to improve agreement with $^{235}U(n,f)$ cross section measurements. The ENDF/B-V.2[20] and ENDF/B-VI[21] evaluated (n,f) cross sections were used to represent the experimental data base. A comparison of our fitted calculation with these evaluated data is given in Fig. 4. The dashed and dotted curves in Fig. 5 illustrate the first-, second-, and third-chance fission contributions. The fission barrier parameters that resulted from the analysis are listed in Table 3

The threshold for second-chance fission of $^{235}U$ occurs near an incident neutron energy of 6 MeV, while third-chance fission becomes important above ~12 MeV. At these energies the major competition to the (n,f) channels comes from (n,xn) reactions. The results of our calculations of the $^{235}U(n,2n)$ and (n,3n) cross sections are compared with the available experimental data[8,22] and with the ENDF/B-V.2 evaluation[20] in Fig. 5. There is reasonable agreement between the calculated and measured (n,2n) cross sections at most energies and similarly for the (n,3n) values below ~15 MeV. At higher energies, however, the calculated (n,3n) cross section rises significantly above the experimental data, reaching about a factor of 2 higher near 20 MeV. It is interesting to note that the theoretical analysis included in Ref. 22 resulted in calculated (n,3n) cross sections that agreed well with experiment but that overpredicted the (n,f) cross section, whereas the converse is true for the present analysis. It might therefore be difficult to reconcile the data in the (n,f) channel with the (n,3n) measurements,[22] although we have not yet made a thorough study of this problem.

## Summary Remarks

The present analysis successfully describes much of the available cross section and angular distribution data for neutron reactions with $^{235}U$ between 0.01 and 20 MeV. Because the analysis is still in progress and additional refinements are possible, the present results should be regarded as preliminary. Any further changes are, however, likely to be small. The final analysis of the (n,n), (n,n'), (n,2n), and (n,3n) cross sections, angular distributions, and emission spectra will be combined at Oak Ridge National Laboratory[23] with a new resonance parameter analysis[24] and with updated evaluations of the fission neutron spectrum and $\nu_p$, the prompt fission neutron multiplicity, for the upcoming ENDF/B-VI evaluation.

## References


1. R. E. Hunter et al., LA-5172 (1973).
2. E. D. Arthur et al., Nucl. Sci. Eng. 88, 56 (1984).
3. J. Q. Shao et al., Nucl. Sci. Eng. 92, 350 (1986).
4. J. Raynal, IAEA SMR-9/8, Int. At. En. Agency (1970).
5. C. M. Perey and F. G. Perey, At. Data and Nucl. Data Tables 17, 1 (1976).
6. G. Haouat et al., Nucl. Sci. Eng. 81, 491 (1982).
7. W. P. Poenitz et al., Nucl. Sci. Eng. 78, 333 (1981).
8. Experimental data available from the CSISRS compilation by the NNDC, Brookhaven National Lab., Upton, N.Y.

9. C. L. Dunford, Ai-AEC-12931, Atomics Int. (1970).

10. P. G. Young and E. D. Arthur, LA-6947 (1977); E. D. Arthur, LA-UR-88-382 (1988).

11. A. Gilbert and A. G. W. Cameron, Can. J. Phys. 43, 1446 (1965).

12. J. L. Cook et al., Aust. J. Phys. 20, 477 (1967).

13. D. M Brink, Nucl. Phys. 4, 215 (1957); P. Axel, Phys. Rev. 126, 671 (1962).

14. A. B. Smith and P. T. Guenther, ANL/NDM-63 (1982); experimental data obtained from Ref. 8.

15. Y. A. Ellis-Akovali, Nucl. Data Sheets 40, 523 (1983); E. N. Shurshikov et al., Nucl. Data Sheets 38, 277 (1983).

16. R. J. Peterson, Ann. Phys. 53, 40 (1969).

17. D. L. Hill and J. A. Wheeler, Phys. Rev. 89, 1102 (1953).

18. H. C. Britt, personal communication (Sept. 1982).

19. S. Bjϕrnholm et al., IAEA-SM-174, V.1 (1974) p. 367.

20. M. R. Bhat, ENDF/B-V, Revision 2 data file for $^{235}$U (MAT 1395), BNL-NCS-17541 (ENDF-201, 3rd Ed., Sup. 1, Jan. 1985).

21. A. D. Carlson et al., Rad. Effects 96, 87 (1986) and personal communication (May 1988).

22. L. R. Veeser and E. D. Arthur, Proc. Int. Conf. on Neut. Phys. and Nucl. Data for Reactors and Other Applied Purposes, Harwell, UK ( September, 1978) p. 1054.

23. L. W. Weston, ORNL, personal communication (May, 1988).

24. H. Derrien et al., ORNL/TM-10098 (1986).

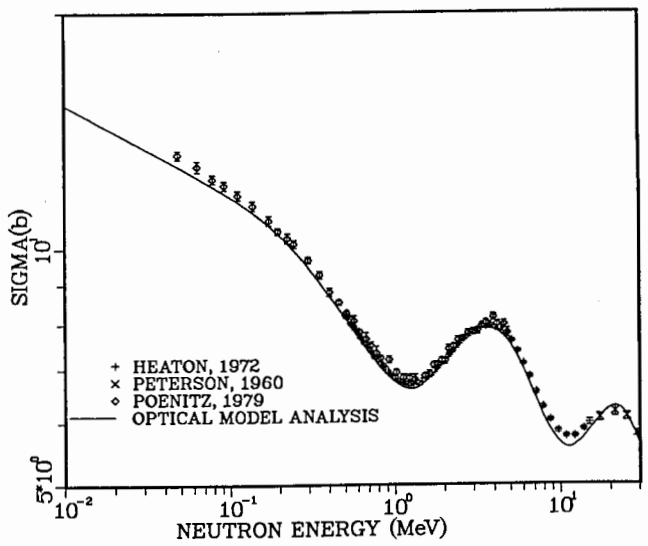


Fig. 1. Measured[8] and calculated neutron total cross section of $^{235}$U.

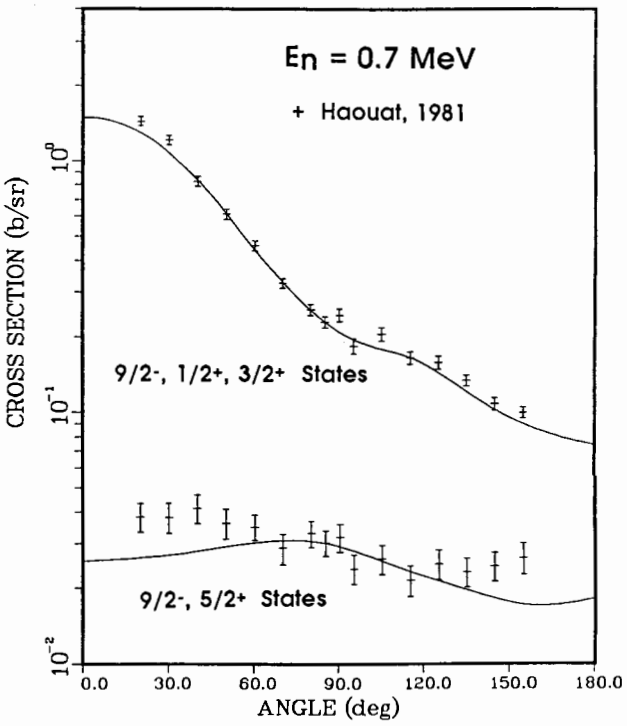


Fig. 2. Measured[6] and calculated neutron scattering cross sections of $^{235}$U at $E_n$ = 0.7 MeV for groups of levels, as indicated. Note that the ground state of $^{235}$U is 7/2-, and the upper curve mainly corresponds to elastic scattering.

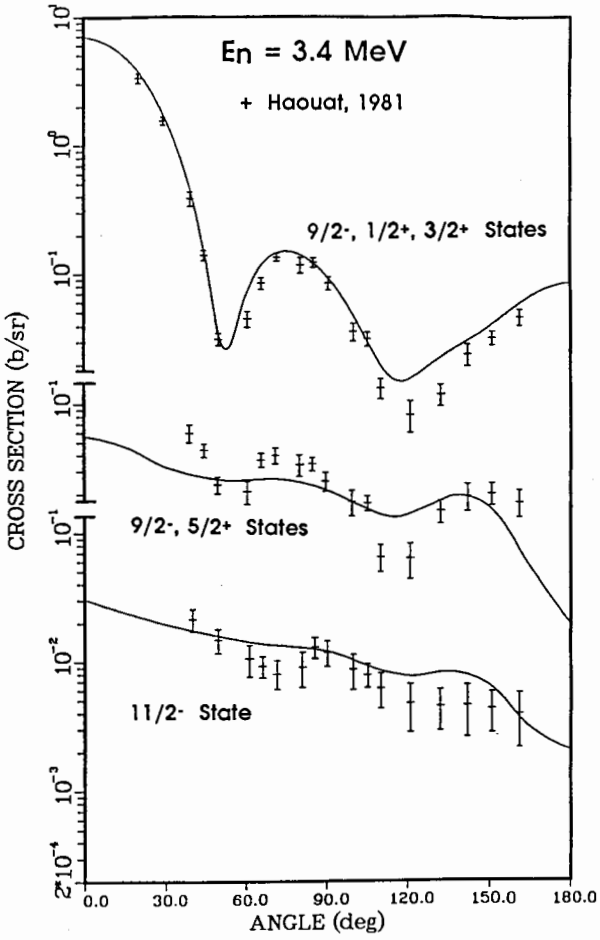


Fig. 3. Measured[6] and calculated neutron scattering cross sections of $^{235}$U at $E_n$ = 3.4 MeV for groups of levels, as indicated. Note that the ground state of $^{235}$U is 7/2-, and the upper curve mainly corresponds to elastic scattering.

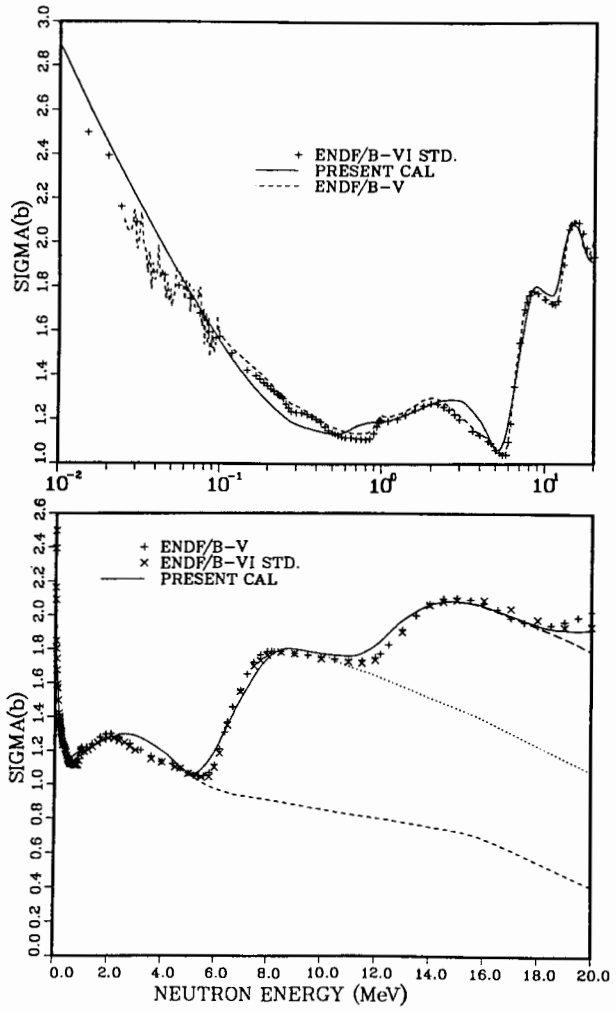


Fig. 4. Comparison of our analysis (smooth curves) of the $^{235}U(n,f)$ cross section with the ENDF/B-V.2[20] and ENDF/B-VI[21] cross section evaluations. The latter evaluation is a standard cross section for ENDF/B-VI. The dashed and dotted curves indicate the contributions from first-, second-, and third-chance fission.

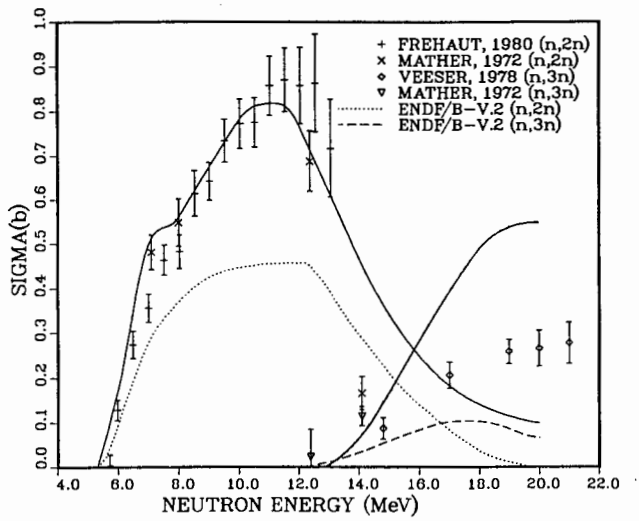


Fig. 5. Measured[8,22] and calculated $^{235}U(n,2n)$ and (n,3n) cross sections. The present analysis is represented by the solid curves, and the ENDF/B-V.2 evaluation is given by the dotted and dashed curves.

Table 1. Optical Model and Deformation Parameters Used in the Calculations*

| Potential | | $r_i$ | $a_i$ |
|---|---|---|---|
| $V = 46.4 - 0.3E$ | | 1.26 | 0.615 |
| $W_{SD} = 3.3 + 0.4E$ | $E \leq 8$ MeV | 1.24 | 0.50 |
| $W_{SD} = 6.5 - 0.046(E-8)$ | $E > 8$ MeV | 1.24 | 0.50 |
| $W_V = -0.7 + 0.1E$ | $E \geq 7$ MeV | 1.26 | 0.63 |
| $V_{SO} = 6.2$ | | 1.12 | 0.47 |

$\beta_2 = 0.215$ $\beta_4 = 0.075$

*The well depths and energies are in MeV; geometric parameters are in fermis. A Woods-Saxon form factor is used throughout.

Table 2. Comparison of Calculated Scattering Cross Sections with the Measurements of Smith and Guenther.[14]

| $E_n$ (MeV) | $E_x$ Range (MeV) | $\sigma_{exp} \pm \Delta\sigma_{exp}$ (barns) | $\sigma_{calc}$ (barns) |
|---|---|---|---|
| 0.93 | 0.0 - 0.09 | 5.02 ± 0.20 | 4.28 |
| 1.27 | 0.0 - 0.12 | 4.13 ± 0.12 | 3.95 |
| 1.49 | 0.0 - 0.13 | 4.11 ± 0.12 | 3.88 |
| 1.85 | 0.0 - 0.13 | 4.23 ± 0.13 | 4.00 |
| 2.55 | 0.0 - 0.30 | 4.55 ± 0.18 | 4.53 |
| 3.55 | 0.0 - 0.30 | 5.14 ± 0.15 | 4.94 |

Table 3. Barrier Parameters Used in Fission Calculations

| | $^{236}U$ | $^{235}U$ | $^{234}U$ | $^{233}U$ |
|---|---|---|---|---|
| $E_A$ (MeV) | 5.57 | 5.73 | 5.50 | 5.50 |
| $\hbar\omega_A$ (MeV) | 0.9 | 0.85 | 0.7 | 0.85 |
| $E_B$ (MeV) | 5.49 | 5.63 | 5.40 | 5.30 |
| $\hbar\omega_B$ (MeV) | 0.5 | 0.55 | 0.5 | 0.55 |
| Density Enhancements: | | | | |
| Barrier A | 2.15 | 2.5 | 1.0 | 5.0 |
| Barrier B | 2.15 | 2.0 | 1.0 | 2.0 |